ACS Partner Journal

Journal of the American Society for Mass Spectrometry

pubs.acs.org/jasms

Research Article

Proteomic Analysis Reveals Low-Dose PARP Inhibitor-Induced Differential Protein Expression in BRCA1-Mutated High-Grade Serous Ovarian Cancer Cells

Jesenia M. Perez, Carly A. I. Twigg, Weihua Guan, and Stefani N. Thomas*

Cite This: *J. Am. Soc. Mass Spectrom.* 2022, 33, 242−250

Read Online

ACCESS | Metrics & More | Article Recommendations | Supporting Information

ABSTRACT: High-grade serous ovarian cancer (HGSOC) is the most common form of ovarian cancer diagnosed in patients worldwide. Patients with *BRCA1/2*-mutated HGSOC have benefited from targeted treatments such as poly(ADP-ribose) polymerase inhibitors (PARPi). Despite the initial success of PARPi-based ovarian cancer treatment regimens, approximately 70% of patients with ovarian cancer relapse and the 5-year survival rate remains at 30%. PARPi exhibit variable treatment efficacy and toxicity profiles. Furthermore, the off-target effects of PARP inhibition have not yet been fully elucidated, warranting further study of these classes of molecules in the context of HGSOC treatment. Highly reproducible quantitative mass spectrometry-based proteomic workflows have been developed for the analysis of tumor tissues and cell lines. To detect the off-target effects of PARP inhibition, we conducted a quantitative mass spectrometry-based proteomic analysis of a *BRCA1*-mutated HGSOC cell line treated with low doses of two PARPi, niraparib and rucaparib. Our goal was to identify PARPi-induced protein signaling pathway alterations toward a more comprehensive elucidation of the mechanism of action of PARPi beyond the DNA damage response pathway. A significant enrichment of nuclear and nucleoplasm proteins that are involved in protein binding was observed in the rucaparib-treated cells. Shared upregulated proteins between niraparib and rucaparib treatment demonstrated RNA II pol promoter-associated pathway enrichment in transcription regulation. Pathway enrichment analyses also revealed off-target effects in the Golgi apparatus and the ER. The results from our mass spectrometry-based proteomic analysis highlights notable off-target effects produced by low-dose treatment of *BRCA1*-mutated HGSOC cells treated with rucaparib or niraparib.

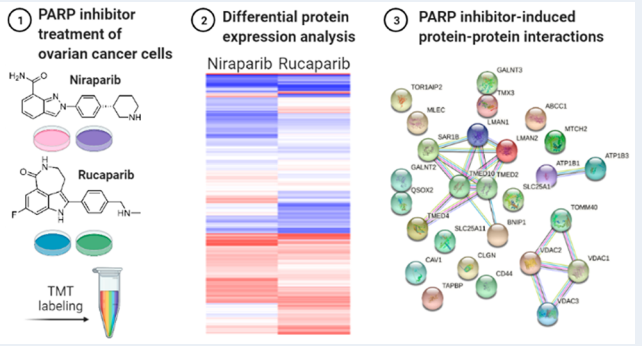

KEYWORDS: *ovarian cancer, tandem mass tags (TMT), mass spectrometry, proteomics, PARP inhibitor (PARPi)*

INTRODUCTION

Epithelial ovarian cancer is the seventh most common cancer, globally, with 239,000 new cases and 152,000 deaths each year.[1,2] Classification of these cancers occurs histologically, and they are divided into five subtypes: high-grade serous (HGS), low-grade serous (LGS), clear cell, endometroid, and mucinous ovarian cancer.[3] High-grade serous ovarian cancer (HGSOC) is the most common form diagnosed in patients worldwide.[4] Diagnosis typically occurs at advanced stages and has poor prognosis because of unspecific symptoms associated with this disease. In addition, there is inadequate screening of early low-volume neoplastic growth.[5] Conventional treatment options for patients with HGSOC include tumor cytoreduction surgery and combination chemotherapy with molecular agents such as cisplatin and paclitaxel; however, a persistent challenge which directly impacts patient survival is disease recurrence.[1,6]

HGSOC is typically characterized by gene abnormalities in *p53* with three frequently altered pathways including RB and PI3K/RAS signaling, NOTCH signaling, and homologous recombination (HR).[7] The HR pathway is altered in up to 51% of HGSOC cases with gene abnormalities in *BRCA1/2*. These abnormalities have been therapeutically exploited via targeted treatments such as poly(ADP-ribose) polymerase (PARP) inhibitors. The PARP family of enzymes function by catalyzing the polymerization of ADP-ribose from NAD^+ molecules to target proteins and are involved in cellular processes including single-stranded break (SSB) and double-stranded break (DSB) repair.[5,8] PARP inhibitors function via competitive inhibition against NAD^+ substrates and lead to inhibition of DNA repair. PARP inhibitors also function by

Received: July 13, 2021
Revised: October 12, 2021
Accepted: October 12, 2021
Published: December 27, 2021

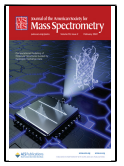

trapping PARP enzymes in DNA damage sites and inhibiting recruitment of other DNA repair proteins.[9] These two processes ultimately lead to genome instability, cell cycle arrest, and cancer cell death.[10] Patients with *BRCA1/2*-mutated cancers have been shown to be deficient in HR and have benefited from PARP inhibitor treatments due to the phenomenon of synthetic lethality wherein two genetic lesions become lethal when combined.[11]

Three PARP inhibitors currently have approval by the U.S. Food and Drug Administration (FDA) for the treatment and maintenance treatment of adult patients with advanced ovarian, fallopian tube, or primary peritoneal cancer with HR-deficient tumors: niraparib, rucaparib, and olaparib. Despite the initial success of PARP inhibitors in the treatment of ovarian cancer, approximately 70% of patients with ovarian cancer relapse with a 30% 5-year survival rate.[2] One factor contributing to this high rate of relapse is the formation of drug resistance. Drug resistance is thought to occur via multiple mechanisms: reactivation of HR in HR-deficient tumors can occur through the accumulation of secondary mutations that restore the open reading frame of *BRCA* genes, replication fork protection through the overexpression of RAD51, and reduced drug uptake via overexpression of MDR1.[12,13] Furthermore, although the current FDA-approved PARP inhibitors have all been shown to prevent PARP activity, their efficacy and toxicities vary.[9] The off-target effects of PARP inhibition have not yet been fully elucidated, warranting further study of these classes of molecules.

Recent advancements in mass spectrometry-based proteomic technologies have enabled the quantification of many types of proteomes, especially in the context of cancer.[14−16] These analytical methods have been used recently to characterize protein changes in cancer cells, leading to functional insights into pathways that are implicated during tumorigenesis or the formation of drug resistance.[17] Highly reproducible quantitative mass spectrometry-based proteomic workflows have been developed for the analysis of tumor tissues and cell lines.[18] Isobaric labeling of peptides with tandem mass tags (TMT) is one such quantitation method.[18,19] Several studies have utilized quantitative mass-spectrometry based proteomics in patient tumor tissue samples and human cell lines to show statistically significant differences in protein regulation, and functional analyses have revealed the enrichment of pathways associated with tumorigenesis.[20,21]

The primary advantage of utilizing a mass spectrometry-based proteomic approach in this context is the ability to identify and quantify changes in the ovarian cancer proteome in an unbiased manner. Specifically, within the context of PARPi treatment, a mass spectrometry-based approach can reveal off-target pathways that are implicated upon PARP inhibition. Recently, PARP inhibitors have been shown to elicit unique polypharmacological properties, a phenomenon where drugs bind to several proteins beyond their intended target.[22−24] TMT labeling followed by mass spectrometry can reveal the underlying mechanisms responsible for these polypharmacological properties, eventually allowing improved patient stratification for PARP inhibitors.

To detect the off-target effects of PARP inhibition, we conducted a quantitative mass spectrometry-based proteomic analysis of a *BRCA1*-mutated HGSOC cell line treated with low doses of two PARP inhibitors, niraparib and rucaparib. Our goal was to identify PARP inhibitor-induced protein signaling pathway alterations toward a more comprehensive elucidation of PARP inhibitors' mechanisms of action beyond the DNA damage response pathway.

MATERIALS AND METHODS

Chemicals and Reagents. Niraparib (MK-4827) and rucaparib (AG-014699) were purchased from Selleck Chemicals. LC/MS-grade water and formic acid were purchased from Fisher Scientific. Anhydrous acetonitrile and iodoacetamide (IAM) were purchased from Millipore Sigma. Lys-C, trypsin, BCA assay kit, DTT, and TMT-10plex Label Reagent were purchased from Thermo Fisher Scientific. The 1 cm^3 C18 SepPak cartridges were purchased from Waters.

COV362 Cell Culture and Lysate Preparation. COV362 cells (ECACC) were incubated at 37 °C in 5% CO_2 in Dulbecco's Modified Eagle medium (DMEM) supplemented with 10% fetal bovine serum (FBS) and 1% penicillin−streptomycin. Cells were seeded at 80% confluency in 10 cm dishes prior to treatment for 8 h in FBS-free medium with 0.5 μM PARP inhibitor (niraparib or rucaparib) dissolved in DMSO. After treatment, cells were washed with ice-cold phosphate-buffered saline (PBS) and collected from each dish using a cell scraper, then centrifuged at 2500*g* at 4 °C for 5 min, washed with PBS, and centrifuged once more. The cell pellets were stored at −80 °C.

Complex IV Activity Assay. Mitochondria were isolated from treated cell pellets using the Mitochondria Isolation Kit for Cultured Cells (Abcam, cat no. ab110170) according to the manufacturer's instructions. Briefly, approximately 4×10^7 cells were ruptured gently using a 1 mL Dounce Homogenizer with a tight pestle, and mitochondria were isolated by differential centrifugation at low speeds (1000*g* for 10 min at 4 °C) followed by high speeds (12000*g* for 15 min at 4 °C). Next, Complex IV activity was assessed from isolated mitochondria using the colorimetric Complex IV Human Specific Activity Microplate Assay Kit (Abcam, cat. no. ab109910). Briefly, this assay determines Complex IV activity via the oxidation of reduced cytochrome c through a decrease in absorbance at 550 nm for 60 min. Complex IV activity was calculated from the rate of enzyme oxidation using the following equation:

$$\text{rate (OD per min)} = \frac{\text{absorbance 1} - \text{absorbance 2}}{\text{time (min)}}$$

Protein Digestion and TMT-Labeling. Cell pellets were resuspended in urea lysis buffer (8 M urea, 75 mM NaCl, 50 mM Tris pH 8.0, 1 mM EDTA, 2 μg/mL aprotinin, 10 μg/mL leupeptin, 1 mM PMSF), vortexed for 10 s, incubated on ice for 15 min, followed by another 10 s vortex and another 15 min incubation on ice. After 20000*g* centrifugation at 4 °C for 10 min, the supernatant was transferred to a new tube and the protein concentration was determined with a BCA protein assay.

For digestion, 50 μg of protein per sample was used for disulfide bond reduction with 50 mM dithiothreitol (DTT) for 1 h at 37 °C and then alkylated with 100 mM iodoacetamide (IAA) for 45 min at room temperature in the dark. The samples were diluted 1:4 with 50 mM Tris (pH 8.0) and subsequently digested with Lys-C at an enzyme/substrate ratio of 1:50 for 1 h with shaking at room temperature, followed by trypsin digest at an enzyme/substrate ratio of 1:50 overnight with shaking at room temperature. The digestion reactions were acidified and quenched with 10% formic acid to a final

https://doi.org/10.1021/jasms.1c00215
J. Am. Soc. Mass Spectrom. 2022, 33, 242−250

concentration of 0.1% followed by centrifugation at 1500*g* for 15 min at room temperature.

The peptide samples were then desalted using 1 cm^3 C18 SepPak cartridges with a vacuum manifold (Waters). The eluates were dried using vacuum centrifugation and reconstituted in 50 mM HEPES pH 8.5 prior to the measurement of peptide concentration with a BCA protein assay. The peptide samples were labeled with TMT-10plex Label Reagent set according to the manufacturer's protocol (Thermo Fisher Scientific). TMT 126 was used as a reference channel, and TMT 127N, 128N, 128C, 129C, 130N, 130C, 127C, and 129N were used to label the four different conditions and their replicates: DMSO with replicate 129C and 128C, niraparib with replicate 130C and 130N, rucaparib with replicate 128N and 127N, and olaparib with replicate 127C and 129N. Each TMT label was reconstituted in 52.5 μL of anhydrous acetonitrile and added at a concentration of 13.3 mM to 16 μg of peptide per sample for 1 h at room temperature and then pooled, desalted, and dried using vacuum centrifugation.

High-pH RPLC Offline Fractionation. The TMT-labeled samples were resuspended in buffer A (20 mM ammonium formate pH 10 in 98:2 water/acetonitrile) prior to high-pH reversed-phase high-performance liquid chromatography (HPLC) fractionation. A Shimadzu Prominance HPLC (Shimadzu) with a Hot Sleeve-25L Column Heater (Analytical Sales & Products, Inc.) was used with a Security Guard precolumn housing a Gemini NX C18 cartridge (Phenomenex) attached to a C18 XBridge column (5 μm particles, 2.1 mm i.d., 150 mm length). The peptides were separated with a gradient of increasing buffer B (20 mM ammonium formate, pH 10 in 10:90 water/acetonitrile) from 2 to 7% over 0.5 min, 7−15% over 7.5 min, 15−35% over 45 min, and 35−60% over 15 min, all at a constant flow rate of 200 μL/min. Fractions were collected every 2 min, and UV absorbances were monitored at 215 and 280 nm where peptide-containing fractions were divided into two equal numbered groups, "early" and "late". A volume equal to 15 milliabsorbance units of the first "early" fraction was concatenated with the first "late" fraction, and so on into 16 concatenated fractions. The concatenated samples were then dried using vacuum centrifugation.

MS Analysis. LC−MS/MS analysis was performed using a nanoflow liquid chromatography system (Dionex Ultimate 3000) coupled with an Orbitrap Fusion MS system (Thermo Fisher). The samples were reconstituted in 2% acetonitrile 0.1% formic acid and injected into a Luna C18 column (20 cm, 5 μm Phenomenex particles, 100 Å pores). Samples were introduced into the mass spectrometer via a 10 μm spray tip (New Objective, i.d. 75 μm, o.d. 360 μm, tip 10 μm). The spray voltage was set to 2100 V. Peptides were separated using a gradient of buffer A (water and 0.1% formic acid) and buffer B (acetonitrile and 0.1% formic acid). The gradient was as follows: 2−10% B over 6 min, 10−35% B over 84 min, 35−80% B over 4 min, at a constant flow rate of 0.3 μL/min. Data were acquired using a top 10 SPS MS^3 method. MS1 scans were acquired in the Orbitrap with a scan range of 350−1800 m/z at a resolution of 120,000 and ions with charges 2+ to 7+ were selected for CID-based MS/MS fragmentation. Dynamic exclusion duration was set to 30 s. MS3 fragmentation was conducted using HCD with a scan range of 100−500 m/z and a resolution of 30,000. The raw mass spectrometry data have been deposited to the ProteomeXchange Consortium via the PRIDE partner repository with the data set identifier PXD027177.[25]

Data Analysis. The MS data were processed using Proteome Discoverer 2.5.0.400 (Thermo Fisher Scientific) and analyzed with SEQUEST HT (Thermo Fisher Scientific) for protein identification using the following parameters: enzyme specificity: trypsin; maximum missed cleavage sites: 2; peptide and fragment mass tolerance: 10 ppm and 0.6 Da, respectively. A SwissProt human database downloaded on 2020-11-23 was used. Static modifications included TMT10-plex at peptide N-termini and TMT10-plex at Lys residues as well as carbamidomethylation of Cys residues. Oxidation of Met and addition of acetyl at the N-termini on each peptide were set as dynamic modifications. Percolator was used to determine the confidence for peptide and protein identification; validation was based on a q value <0.05, and a strict false discovery rate (FDR) target was set to 0.01. Protein grouping was conducted according to the principle of maximum parsimony. For protein and peptide quantification, the peak integration tolerance of "Reporter Ions Quantifier" was set to 20 ppm. Reporter ions 126, 129C, 128C, 130C, 130N, 128N, 127N, 127C, and 129N were detected.

Proteomic data were filtered based on the following parameters for proteins: high protein FDR confidence, grouped abundances in every sample: >0, ≥2 unique peptides per protein. The following parameters were set for peptide groups: confidence: high, grouped abundances in every sample: >0, PSM ambiguity: unambiguous, and each peptide group belongs to one protein group. Following data filtering, data were exported to Excel where proteins without associated peptides or proteins with only one quantified peptide were manually removed from the data set. Next, raw peptide intensities were Log_2 transformed and normalized based on the median value of each treatment condition for each sample. CVs were calculated from the median-normalized log_2 transformed intensities per treatment and peptides with CVs greater than 30% were removed from the data set. The median peptide abundance per protein was then calculated and divided by the protein abundance of the reference channel to normalize and correct for intrarun variability. Then, a protein matrix was generated for further analysis (Supporting Table 1). The transformation and normalization of our data was done such that overall protein abundance was approximately normally distributed for downstream statistical analysis. In a data set that is normally distributed, a z-score of ±1.96 is representative of a p-value that is <0.05 and represents significantly upregulated or downregulated protein abundance.

The Database for Annotation, Visualization, and Integrated Discovery (DAVID) was used to analyze proteins that were differentially expressed in each treatment condition as determined by a one-tail Fisher Exact probability value for gene-enrichment analysis.[26,27] The DAVID default *Homo sapiens* background genome was used for functional annotation analysis. Biological processes, cellular components, molecular functions, and pathways that were significantly enriched (p-value < 0.01) were analyzed using DAVID's clustering algorithm which classifies highly related genes into functionally related groups. Proteins were further analyzed using STRING to investigate functional protein association networks. The confidence level for the strength of the association between proteins in STRING analysis was set to the highest strength. This setting decreased coverage but included identified proteins that were more likely to be true positives.[28]

https://doi.org/10.1021/jasms.1c00215
J. Am. Soc. Mass Spectrom. 2022, 33, 242−250

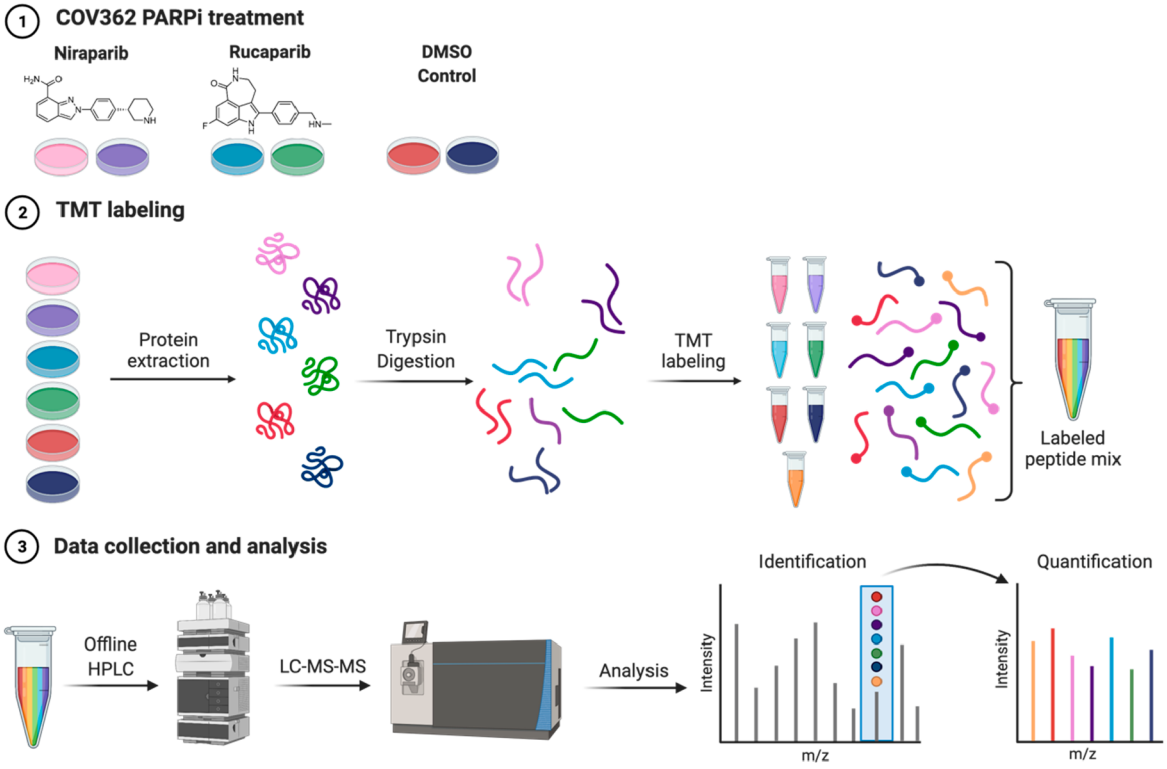

Figure 1. Experimental scheme for the treatment of high-grade serous ovarian cancer cells, COV362, with PARP inhibitors. Cells were treated with 0.5 μM niraparib or rucaparib for 8 h in serum-free medium. Following treatment, proteins were extracted and digested for 15 h with trypsin and LysC prior to TMT labeling. Samples were then fractionated using offline bRPLC and concatenated for LC−MS/MS analysis. Created with BioRender.com.

RESULTS AND DISCUSSION

Workflow for the Identification and Quantification of Proteins in PARPi-Treated Cells. To identify and quantify differential protein expression in PARPi-treated ovarian cancer cells, COV362 cells were treated with 0.5 μM niraparib or rucaparib for 8 h under serum-free medium conditions prior to harvesting, TMT labeling, fractionation, and MS analysis (Figure 1). Four conditions (niraparib, rucaparib, and olaparib) were tested, however, due to high technical variation in the olaparib treatment conditions (where the CV was >30%) this treatment was omitted from further analysis. The half maximal inhibitory concentrations (IC_{50}) of niraparib or rucaparib for COV362 cells are not known. However, according to the Genomics of Drug Sensitivity in Cancer (GDSC) database (https://www.cancerrxgene.org/), the IC_{50} values of Niraparib following treatment in a panel of 21 ovarian cancer cell lines ranges between 16.7 and 1280 μM. The IC_{50} values of rucaparib following treatment in a panel of 33 ovarian cancer cell lines ranges between 4.21 and 315 μM.[29] Given these broad ranges, a minimal dose of 0.5 μM of PARPi treatment was used to assess the effects of low-dose PARPi treatment on the proteome of HGSOC cells and to elucidate potential resistance mechanisms that may arise from treatment with sup-optimal drug concentrations. COV362 cells were chosen for this study because they serve as a representative model of high-grade serous ovarian cancer (HGSOC) with characteristics of high colony formation, resistance to cisplatin, and *BRCA1* mutational status.[30] Following protein extraction and trypsin digestion, PARPi-treated samples were labeled using six channels from a 10-plex TMT, and a reference channel with all samples combined was generated to enable interset normalization. The six channels within the 10-plex are as follows: two channels per drug treatment (rucaparib and niraparib) which include technical replicates and two channels for DMSO-treated cells. To enable comprehensive global proteome analysis, the labeled peptide mix was fractionated and concatenated prior to MS analysis. Next, peptides were identified and quantified using an SPS MS^3 method. In total, 41,507 peptide groups corresponding to 5026 proteins were quantified across all six treatment conditions using this approach after filtering based on CVs < 30% (Supporting Table 1).

COV362 Cells Treated with Niraparib or Rucaparib Show Differences in Protein Expression. Even though PARPi have been shown to be effective in cancers with *BRCA* mutations via synthetic lethality, the majority of *BRCA* mutant patients do not show favorable responses to therapy and they develop resistance.[31] Recent studies have attempted to outline gene expression signatures that predict response to PARPi using algorithms that make predictions using solid tumor cell lines and patient samples based on features such as the BRCAness signature, the PARP sensitivity signature, and HRD Score.[32−34] These efforts have resulted in discovering that PARPi response is dependent on gene interactions that affect the HR pathway.[32] However, little is known about the off-target pathways implicated by PARP inhibition.

Here, we used an unbiased mass spectrometry-based proteomic approach to further elucidate the effect of low-dose PARPi on the global cellular proteome. Following the identification and quantification of the proteins in each PARPi-treated sample, z-scores were calculated, and relative protein abundances were visualized using a heatmap (Figure 2A).

https://doi.org/10.1021/jasms.1c00215
J. Am. Soc. Mass Spectrom. 2022, 33, 242−250

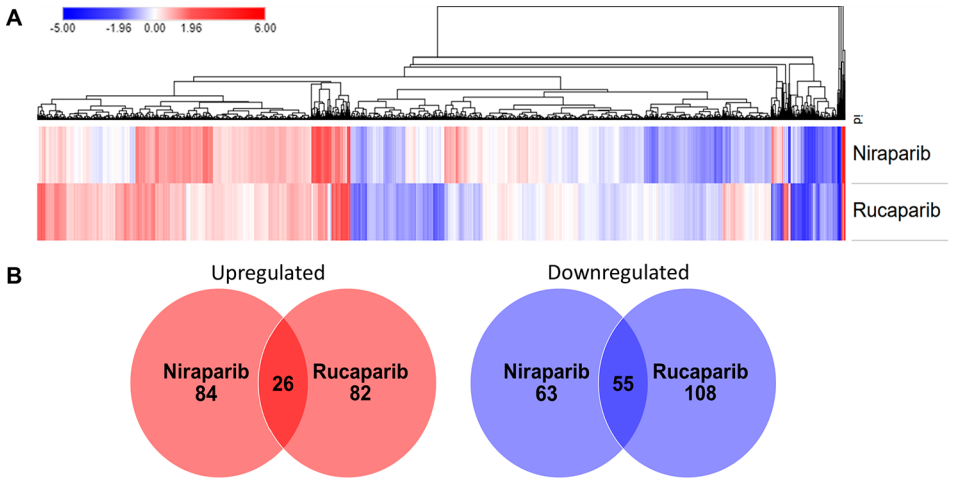

Figure 2. COV362 cells treated with different PARPi have unique protein expression profiles. (A) Heatmap of protein expression in cells treated with 0.5 μM niraparib or rucaparib relative to control (DMSO). Protein expression z-scores were calculated from relative abundances from 5026 proteins, and Euclidean distance clustering was used to construct the heatmap; blue and red areas represent downregulation and upregulation of protein expression, respectively. (B) Venn diagram of the number of significantly upregulated and downregulated proteins with relative abundances $\pm$1.962 standard deviations.

COV362 cells treated with rucaparib had 63 downregulated proteins, while cells treated with Niraparib had 84 upregulated proteins. Overall, 192 proteins were significantly upregulated as determined by having a z-score greater than 1.962 standard deviations following PARPi treatment, while 226 proteins were significantly downregulated with z-scores less than −1.962 standard deviations (Figure 2B).

Rucaparib and niraparib have similar relative PARP-trapping capacities, but in the context of clinical treatment efficacy, they differ with respect to the most frequent toxicities experienced by patients. For example, approximately 34% of patients treated with niraparib suffer from thrombocytopenia.[35] This phenomenon is largely not observed in patients treated with rucaparib. The treatment regimens of these PARPi are not identical. In addition, the cytotoxic potential of FDA-approved PARPi differs between HR-deficient (HRD) and HR-proficient cell lines. Finally, rucaparib inhibits a subset of CYP2 enzymes, a family of enzymes involved in drug metabolism, whereas niraparib inhibits MATE1/2, a protein involved in drug efflux.[36,37]

The significant differences in protein expression that we observed in our study upon niraparib or rucaparib treatment indicate that PARPi have different off-target effects beyond the DNA damage response pathway. Recent studies have demonstrated that PARPi, including rucaparib and niraparib, have unique off-target effects on various kinase families at submicromolar doses; niraparib was found to inhibit DYRK1A/B, while rucaparib inhibited CDK16, PIM3, and DYRK1B.[22,36] Another study found that PARPi demonstrated antitumor efficacy through PARP-independent mechanisms in triple negative breast cancer cells.[38] These unique off-target effects leading to differential protein expression may potentially contribute to the development of specific drug resistance mechanisms.

Niraparib and Rucaparib Have Unique off-Target Effects in COV362 Cells. Proteins that were significantly upregulated or downregulated following PARPi treatments were further analyzed using DAVID. Here, the cellular compartments, molecular functions, and biological processes of each protein that was enriched in COV362 cells post-treatment were investigated. Cells treated with rucaparib had a significant enrichment of proteins found within the nucleus and nucleoplasm that are involved in protein binding (Figure 3A). In addition, DAVID analysis showed an enrichment of biological processes that included DNA recombination and termination of RNA pol II transcription. Functional protein association network analysis performed by STRING predicted interactions between the THO complex, SRSF1, and SNRPE (Figure 3B). The THO complex functions in mRNP biogenesis and is implicated in tumorigenesis; a semi-quantitative immunohistochemistry approach demonstrated high expression of Thoc1 in low- and high-grade ovarian tumor tissue.[39] SRSF1 and SNRPE are involved in mRNA splicing, they are upregulated in many cancers, and they are involved in mTOR activation and regulation.[40,41] Notably, the expression of these proteins was upregulated only in cells treated with rucaparib, indicating an interaction between rucaparib and mRNA processing.

Interestingly, RBBP4 and NHEJ1, factors involved in chromatin reassembly and DNA damage repair, were also enriched in COV362 cells upon treatment with rucaparib. This particular finding supports the proposed function of PARPi in *BRCA1*-mutated cells, where the NHEJ pathway is selected and leads to erroneous repair of damaged DNA, thus leading to genome instability and cancer cell death.[5] Moreover, pathway enrichment analysis revealed many significantly downregulated proteins that are involved in oxidative phosphorylation, mitochondrial translational termination, and mitochondrial translational elongation (Figure 3C). Downregulated proteins involved in these pathways include mitochondrial ribosomal protein (MRPLs), NDUs, and UQCRQ (Figure 3D). Interestingly, PARPi has been shown to provide mitochondria with protection from reactive oxygen species (ROS). In the presence of oxidative stress, PARP1 becomes activated, leads to NAD+ and ATP depletion and contributes to cell death.[42] However, upon PARP inhibition during oxidative stress conditions, mitochondria are rescued from ROS damage through activation of Akt, which interacts with the mTOR and NEMO complex, forming a signalosome which is hypothesized to be involved in maintaining mitochondrial

https://doi.org/10.1021/jasms.1c00215
J. Am. Soc. Mass Spectrom. 2022, 33, 242−250

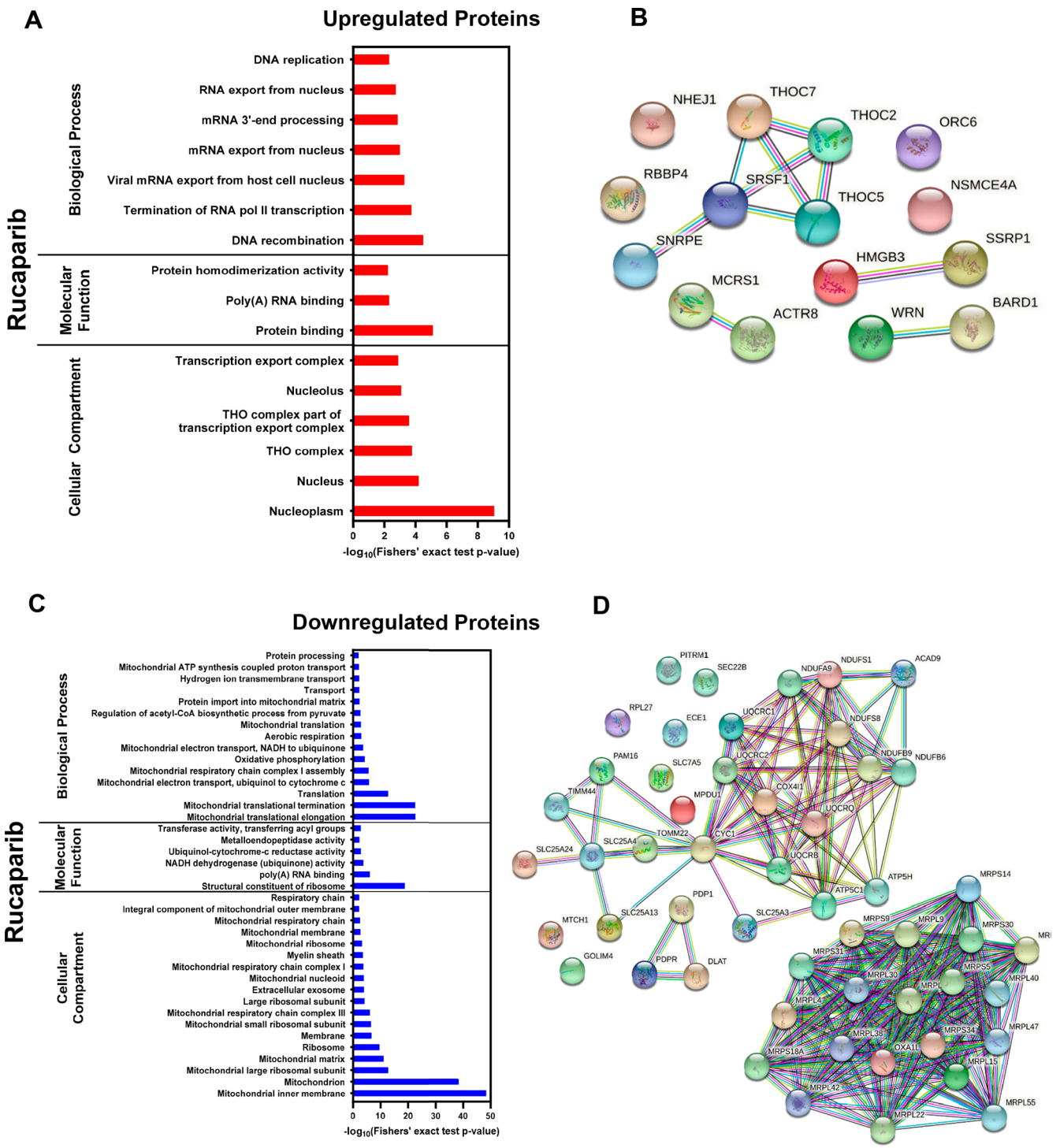

Figure 3. Identification of enriched pathways reveal that PARPi have distinct off-target effects in COV362 cells. DAVID analysis was used to identify cellular compartments, molecular functions, and biological processes that are enriched in COV362 cells following rucaparib treatment. Pathway analysis of proteins that are upregulated (A) or downregulated (C) in cells treated with rucaparib, p-value <0.01. Functional protein association network analysis performed by STRING with proteins upregulated (B) or downregulated (D) following rucaparib treatment; edges represent protein−protein associations between each node with a minimum required interaction score of 0.9000 (high confidence).

integrity.[43] These findings contrast with ours; varying protein levels of Akt, ATM, and the NEMO complex were not found through our proteomic analysis of downregulated proteins after low-dose PARPi treatment, indicating that PARP inhibition at low doses may not be cytoprotective and is involved in mitochondrial dysfunction in HGSOC. To assess the role of PARPi, specifically rucaparib, in inducing mitochondrial dysfunction, Complex IV activity was assessed in treated cells (Figure 4). Proteins that comprise Complex IV in the mitochondria such as COX4I1, were found to be significantly downregulated in rucaparib-treated cells following our initial proteomic analysis. We hypothesized that a decrease in Complex IV activity would occur following rucaparib treatment. Our results do not demonstrate a significant difference

https://doi.org/10.1021/jasms.1c00215
J. Am. Soc. Mass Spectrom. 2022, 33, 242−250

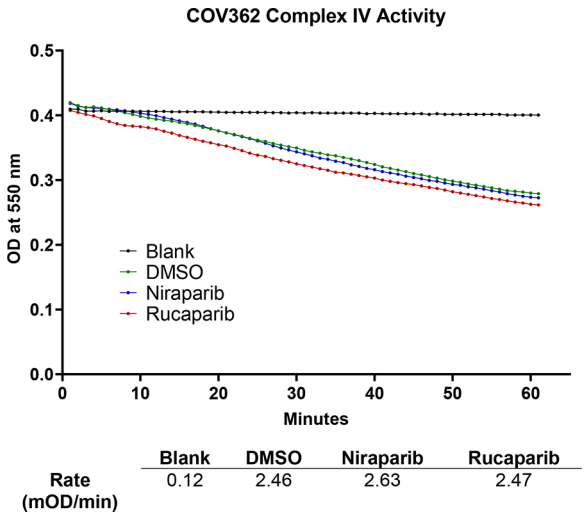

Figure 4. Assessment of complex IV activity in COV362 cells treated with niraparib or rucaparib. Complex IV activity was assessed in treated cells by measuring the oxidation of cytochrome c as a decrease in absorbance at 550 nm and calculating the rate as mOD per minute.

in Complex IV activity between the untreated and PARPi-treated cells; however, this lack of significant difference may be due to low-dose treatment. In addition, these results demonstrate that the effects of PARPi are likely involved in a complex network of regulation beyond Complex IV activity.

Conversely, COV362 cells treated with niraparib had less specific enrichment of biological processes for upregulated and downregulated proteins; however, this may be due in part to the low dosage administered to cells, which is a limitation of this study (Supporting Figure 2).

Despite the differences in upregulated or downregulated proteins in PARPi-treated cells, both PARPi resulted in the significant downregulation of 55 proteins (Figure 2B). Further functional analyses of these proteins revealed an enrichment in biological processes encompassing vesicle-mediated transport between the ER and Golgi body (Figure 5A). Proteins predicted to be involved in these processes include LMAN, TMED, and SAR1B (Figure 5B). To our knowledge, the role of PARPi in vesicle-mediated intracellular transport has not been established; however, this pathway could be involved in mechanisms associated with drug resistance. Exosomes (originating from endosomes formed by the Golgi and ER network) containing noncoding miRNAs secreted by tumor cells have been shown to lead to multidrug resistance in different cancers.[44] Conversely, shared upregulated proteins between the niraparib- and rucaparib-treated cells demonstrated pathway enrichment in transcription regulation from the RNA II pol promoter, indicating the activation of pathways associated with PARPi treatment (Supporting Figure 2).

The results from our mass spectrometry-based proteomic analysis highlight notable off-target effects produced by a low-dose treatment of rucaparib or niraparib. To further elucidate the roles of PARPi treatment in implicating other pathways besides DNA damage in a physiologically relevant manner, future studies will entail the treatment of HGSOC cell lines at clinically relevant PARPi doses. In addition, using a panel of

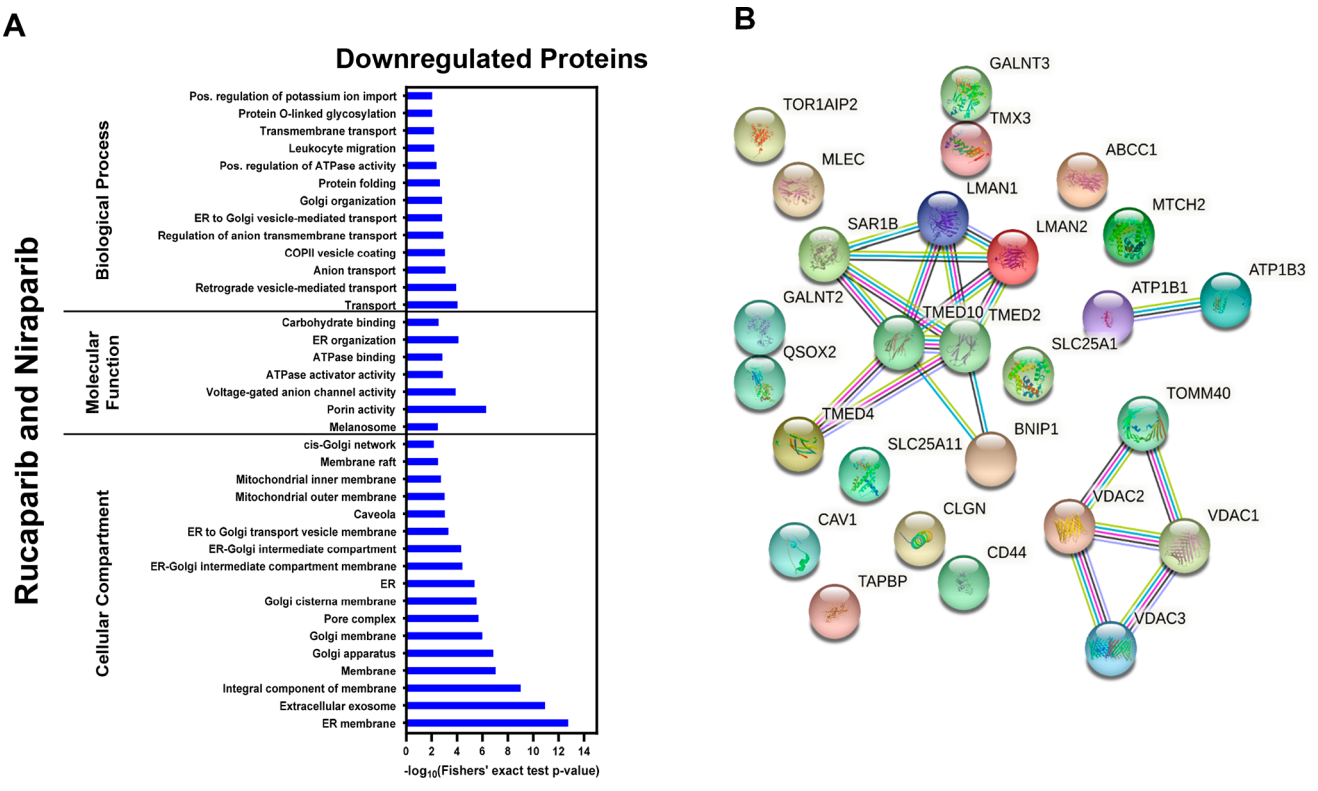

Figure 5. Pathway enrichment analyses reveals low-dose treatment with niraparib or rucaparib induces off-target effects in the Golgi apparatus and the ER. Analysis of enriched pathways in downregulated proteins shared between niraparib- and rucaparib-treated COV362 cells. (A) Downregulated proteins found in both niraparib- and rucaparib-treated COV362 cells, p-value <0.01. (B) Functional protein association network analysis performed by STRING with downregulated proteins shared between cells treated with rucaparib or niraparib; edges represent protein−protein associations between each node with minimum required interaction score being the highest confidence (0.9000).

https://doi.org/10.1021/jasms.1c00215
J. Am. Soc. Mass Spectrom. 2022, 33, 242−250

HGSOC cell lines with unique *BRCA1/2* mutations could provide insight into the functional mechanisms associated with the broad spectrum of patient responsiveness to PARPi treatment.

CONCLUSION

In conclusion, we used a quantitative mass spectrometry-based proteomic approach to identify PARP inhibitor-induced protein signaling pathway alterations in a *BRCA1*-mutated HGSOC cell line. We demonstrated that COV362 cells treated with low-dose niraparib or rucaparib had unique protein expression profiles. Furthermore, cells treated with rucaparib had notable off-target effects. Proteins associated with mitochondrial function were downregulated, indicating a certain degree of mitochondrial dysfunction even with a low dose of rucaparib. Conversely, rucaparib-treated cells had increased expression of proteins associated with mRNA processing. Finally, pathway enrichment analysis revealed a downregulation of proteins involved in Golgi and ER function. In summary, we present unique, off-target pathways that are implicated by niraparib- or rucaparib-mediated PARP inhibition. Future studies will utilize a panel of HGSOC cell lines harboring varying *BRCA1/2* mutational statuses and treated with clinically relevant doses of the three FDA-approved PARP inhibitors for HGSOC.

ASSOCIATED CONTENT

Supporting Information

The Supporting Information is available free of charge at https://pubs.acs.org/doi/10.1021/jasms.1c00215.

Supplemental tables and figures (PDF)

Proteomic data matrix with protein and peptide grouped abundances (XLSX)

AUTHOR INFORMATION

Corresponding Author

Stefani N. Thomas − *Department of Laboratory Medicine and Pathology, University of Minnesota School of Medicine, Minneapolis, Minnesota 55455, United States;* orcid.org/0000-0003-1679-5453; Phone: 612-624-1054; Email: stefanit@umn.edu

Authors

Jesenia M. Perez − *Microbiology, Immunology, and Cancer Biology Graduate Program, University of Minnesota School of Medicine, Minneapolis, Minnesota 55455, United States;* orcid.org/0000-0002-1566-530X

Carly A. I. Twigg − *Department of Laboratory Medicine and Pathology, University of Minnesota School of Medicine, Minneapolis, Minnesota 55455, United States*

Weihua Guan − *Division of Biostatistics, University of Minnesota School of Public Health, Minneapolis, Minnesota 55455, United States*

Complete contact information is available at: https://pubs.acs.org/10.1021/jasms.1c00215

Notes

The authors declare no competing financial interest.

ACKNOWLEDGMENTS

Mass spectrometry data were acquired in the Analytical Biochemistry Shared Resource of the University of Minnesota Masonic Cancer Center, supported in part by the National Cancer Institute (Cancer Center Support Grant No. CA-77598). S.N.T. acknowledges funding from the National Institutes of Health's National Center for Advancing Translational Sciences, Grant No. UL1TR002494, via the University of Minnesota's Clinical and Translational Science Institute. S.N.T. also acknowledges funding from the V Foundation from Cancer Research and startup funds provided by the University of Minnesota Department of Laboratory Medicine and Pathology.

REFERENCES

(1) Lheureux, S.; Braunstein, M.; Oza, A. M. Epithelial ovarian cancer: Evolution of management in the era of precision medicine. *Ca-Cancer J. Clin.* **2019**, *69*, 280−304.

(2) Siegel, R. L.; Miller, K. D.; Fuchs, H. E.; Jemal, A. Cancer Statistics, 2021. *Ca-Cancer J. Clin.* **2021**, *71*, 7−33.

(3) Jelovac, D.; Armstrong, D. K. Recent progress in the diagnosis and treatment of ovarian cancer. *Ca-Cancer J. Clin.* **2011**, *61*, 183−203.

(4) Prat, J. Ovarian carcinomas: five distinct diseases with different origins, genetic alterations, and clinicopathological features. *Virchows Arch.* **2012**, *460*, 237−249.

(5) Konecny, G. E.; Kristeleit, R. S. PARP inhibitors for BRCA1/2-mutated and sporadic ovarian cancer: current practice and future directions. *Br. J. Cancer* **2016**, *115*, 1157−1173.

(6) Lisio, M. A.; Fu, L.; Goyeneche, A.; Gao, Z. H.; Telleria, C. High-Grade Serous Ovarian Cancer: Basic Sciences, Clinical and Therapeutic Standpoints. *Int. J. Mol. Sci.* **2019**, *20*, 952.

(7) Jayson, G. C.; Kohn, E. C.; Kitchener, H. C.; Ledermann, J. A. Ovarian cancer. *Lancet* **2014**, *384*, 1376−1388.

(8) Kim, M. Y.; Zhang, T.; Kraus, W. L. Poly(ADP-ribosyl)ation by PARP-1: 'PAR-laying' NAD+ into a nuclear signal. *Genes Dev.* **2005**, *19*, 1951−1967.

(9) LaFargue, C. J.; Dal Molin, G. Z.; Sood, A. K.; Coleman, R. L. Exploring and comparing adverse events between PARP inhibitors. *Lancet Oncol.* **2019**, *20*, e15−e28.

(10) Rabenau, K.; Hofstatter, E. DNA Damage Repair and the Emerging Role of Poly(ADP-ribose) Polymerase Inhibition in Cancer Therapeutics. *Clin. Ther.* **2016**, *38*, 1577−1588.

(11) Lord, C. J.; Ashworth, A. PARP inhibitors: Synthetic lethality in the clinic. *Science* **2017**, *355*, 1152−1158.

(12) McMullen, M.; Karakasis, K.; Madariaga, A.; Oza, A. M. Overcoming Platinum and PARP-Inhibitor Resistance in Ovarian Cancer. *Cancers* **2020**, *12*, 1607.

(13) Freimund, A. E.; Beach, J. A.; Christie, E. L.; Bowtell, D. D. L. Mechanisms of Drug Resistance in High-Grade Serous Ovarian Cancer. *Hematol Oncol Clin North Am.* **2018**, *32*, 983−996.

(14) Bandu, R.; Oh, J. W.; Kim, K. P. Mass spectrometry-based proteome profiling of extracellular vesicles and their roles in cancer biology. *Exp. Mol. Med.* **2019**, *51*, 1−10.

(15) Swiatly, A.; Plewa, S.; Matysiak, J.; Kokot, Z. J. Mass spectrometry-based proteomics techniques and their application in ovarian cancer research. *J. Ovarian Res.* **2018**, *11*, 88.

(16) Nusinow, D. P.; Szpyt, J.; Ghandi, M.; Rose, C. M.; McDonald, E. R.; Kalocsay, M.; Jané-Valbuena, J.; Gelfand, E.; Schweppe, D. K.; Jedrychowski, M.; Golji, J.; Porter, D. A.; Rejtar, T.; Wang, Y. K.; Kryukov, G. V.; Stegmeier, F.; Erickson, B. K.; Garraway, L. A.; Sellers, W. R.; Gygi, S. P. Quantitative Proteomics of the Cancer Cell Line Encyclopedia. *Cell* **2020**, *180*, 387−402.

(17) Ryu, J.; Thomas, S. N. Quantitative Mass Spectrometry-Based Proteomics for Biomarker Development in Ovarian Cancer. *Molecules* **2021**, *26*, 2674.

(18) Mertins, P.; Tang, L. C.; Krug, K.; Clark, D. J.; Gritsenko, M. A.; Chen, L.; Clauser, K. R.; Clauss, T. R.; Shah, P.; Gillette, M. A.; Petyuk, V. A.; Thomas, S. N.; Mani, D. R.; Mundt, F.; Moore, R. J.; Hu, Y.; Zhao, R.; Schnaubelt, M.; Keshishian, H.; Monroe, M. E.; Zhang, Z.; Udeshi, N. D.; Mani, D.; Davies, S. R.; Townsend, R. R.;

Chan, D. W.; Smith, R. D.; Zhang, H.; Liu, T.; Carr, S. A. Reproducible workflow for multiplexed deep-scale proteome and phosphoproteome analysis of tumor tissues by liquid chromatography-mass spectrometry. *Nat. Protoc.* **2018**, *13*, 1632−1661.
(19) Rauniyar, N.; Yates, J. R. Isobaric labeling-based relative quantification in shotgun proteomics. *J. Proteome Res.* **2014**, *13*, 5293−5309.
(20) Mukherjee, A.; Chiang, C. Y.; Daifotis, H. A.; Nieman, K. M.; Fahrmann, J. F.; Lastra, R. R.; Romero, I. L.; Fiehn, O.; Lengyel, E. Adipocyte-Induced FABP4 Expression in Ovarian Cancer Cells Promotes Metastasis and Mediates Carboplatin Resistance. *Cancer Res.* **2020**, *80*, 1748−1761.
(21) Zhang, W.; Ou, X.; Wu, X. Proteomics profiling of plasma exosomes in epithelial ovarian cancer: A potential role in the coagulation cascade, diagnosis and prognosis. *Int. J. Oncol.* **2019**, *54*, 1719−1733.
(22) Antolin, A. A.; Ameratunga, M.; Banerji, U.; Clarke, P. A.; Workman, P.; Al-Lazikani, B. The kinase polypharmacology landscape of clinical PARP inhibitors. *Sci. Rep.* **2020**, *10*, 2585.
(23) Makhov, P.; Uzzo, R. G.; Tulin, A. V.; Kolenko, V. M. Histone-dependent PARP-1 inhibitors: A novel therapeutic modality for the treatment of prostate and renal cancers. *Urol Oncol.* **2021**, *39*, 312−315.
(24) Passeri, D.; Camaioni, E.; Liscio, P.; Sabbatini, P.; Ferri, M.; Carotti, A.; Giacchè, N.; Pellicciari, R.; Gioiello, A.; Macchiarulo, A. Concepts and Molecular Aspects in the Polypharmacology of PARP-1 Inhibitors. *ChemMedChem* **2016**, *11*, 1219−1226.
(25) Perez-Riverol, Y.; Csordas, A.; Bai, J.; Bernal-Llinares, M.; Hewapathirana, S.; Kundu, D. J.; Inuganti, A.; Griss, J.; Mayer, G.; Eisenacher, M.; Pérez, E.; Uszkoreit, J.; Pfeuffer, J.; Sachsenberg, T.; Yilmaz, S.; Tiwary, S.; Cox, J.; Audain, E.; Walzer, M.; Jarnuczak, A. F.; Ternent, T.; Brazma, A.; Vizcaíno, J. A. The PRIDE database and related tools and resources in 2019: improving support for quantification data. *Nucleic Acids Res.* **2019**, *47*, D442−D450.
(26) Huang, d.W.; Sherman, B. T.; Lempicki, R. A. Bioinformatics enrichment tools: paths toward the comprehensive functional analysis of large gene lists. *Nucleic Acids Res.* **2009**, *37*, 1−13.
(27) Huang, d.W.; Sherman, B. T.; Lempicki, R. A. Systematic and integrative analysis of large gene lists using DAVID bioinformatics resources. *Nat. Protoc.* **2009**, *4*, 44−57.
(28) Szklarczyk, D.; Gable, A. L.; Lyon, D.; Junge, A.; Wyder, S.; Huerta-Cepas, J.; Simonovic, M.; Doncheva, N. T.; Morris, J. H.; Bork, P.; Jensen, L. J.; Mering, C. V. STRING v11: protein-protein association networks with increased coverage, supporting functional discovery in genome-wide experimental datasets. *Nucleic Acids Res.* **2019**, *47*, D607−D613.
(29) Yang, W.; Soares, J.; Greninger, P.; Edelman, E. J.; Lightfoot, H.; Forbes, S.; Bindal, N.; Beare, D.; Smith, J. A.; Thompson, I. R.; Ramaswamy, S.; Futreal, P. A.; Haber, D. A.; Stratton, M. R.; Benes, C.; McDermott, U.; Garnett, M. J. Genomics of Drug Sensitivity in Cancer (GDSC): a resource for therapeutic biomarker discovery in cancer cells. *Nucleic Acids Res.* **2012**, *41*, D955−961.
(30) Haley, J.; Tomar, S.; Pulliam, N.; Xiong, S.; Perkins, S. M.; Karpf, A. R.; Mitra, S.; Nephew, K. P.; Mitra, A. K. Functional characterization of a panel of high-grade serous ovarian cancer cell lines as representative experimental models of the disease. *Oncotarget.* **2016**, *7*, 7.
(31) Brown, J. S.; Kaye, S. B.; Yap, T. A. PARP inhibitors: the race is on. *Br. J. Cancer* **2016**, *114*, 713−715.
(32) McGrail, D. J.; Lin, C. C.; Garnett, J.; Liu, Q.; Mo, W.; Dai, H.; Lu, Y.; Yu, Q.; Ju, Z.; Yin, J.; Vellano, C. P.; Hennessy, B.; Mills, G. B.; Lin, S. Y. Improved prediction of PARP inhibitor response and identification of synergizing agents through use of a novel gene expression signature generation algorithm. *NPJ. Syst. Biol. Appl.* **2017**, *3*, 8.
(33) Konstantinopoulos, P. A.; Spentzos, D.; Karlan, B. Y.; Taniguchi, T.; Fountzilas, E.; Francoeur, N.; Levine, D. A.; Cannistra, S. A. Gene expression profile of BRCAness that correlates with responsiveness to chemotherapy and with outcome in patients with epithelial ovarian cancer. *J. Clin. Oncol.* **2010**, *28*, 3555−3561.
(34) Peng, G.; Chun-Jen Lin, C.; Mo, W.; Dai, H.; Park, Y. Y.; Kim, S. M.; Peng, Y.; Mo, Q.; Siwko, S.; Hu, R.; Lee, J. S.; Hennessy, B.; Hanash, S.; Mills, G. B.; Lin, S. Y. Genome-wide transcriptome profiling of homologous recombination DNA repair. *Nat. Commun.* **2014**, *5*, 3361.
(35) Pilié, P. G.; Gay, C. M.; Byers, L. A.; O'Connor, M. J.; Yap, T. A. PARP Inhibitors: Extending Benefit Beyond. *Clin. Cancer Res.* **2019**, *25*, 3759−3771.
(36) Longoria, T. C.; Tewari, K. S. Pharmacokinetic drug evaluation of niraparib for the treatment of ovarian cancer. *Expert Opin. Drug Metab. Toxicol.* **2018**, *14*, 543−550.
(37) Parkes, E. E.; Kennedy, R. D. Clinical Application of Poly(ADP-Ribose) Polymerase Inhibitors in High-Grade Serous Ovarian Cancer. *Oncologist* **2016**, *21*, 586−593.
(38) Chuang, H. C.; Kapuriya, N.; Kulp, S. K.; Chen, C. S.; Shapiro, C. L. Differential anti-proliferative activities of poly(ADP-ribose) polymerase (PARP) inhibitors in triple-negative breast cancer cells. *Breast Cancer Res. Treat.* **2012**, *134*, 649−659.
(39) Domínguez-Sánchez, M. S.; Sáez, C.; Japón, M. A.; Aguilera, A.; Luna, R. Differential expression of THOC1 and ALY mRNP biogenesis/export factors in human cancers. *BMC Cancer* **2011**, *11*, 77.
(40) Das, S.; Krainer, A. R. Emerging functions of SRSF1, splicing factor and oncoprotein, in RNA metabolism and cancer. *Mol. Cancer Res.* **2014**, *12*, 1195−1204.
(41) Quidville, V.; Alsafadi, S.; Goubar, A.; Commo, F.; Scott, V.; Pioche-Durieu, C.; Girault, I.; Baconnais, S.; Le Cam, E.; Lazar, V.; Delaloge, S.; Saghatchian, M.; Pautier, P.; Morice, P.; Dessen, P.; Vagner, S.; André, F. Targeting the deregulated spliceosome core machinery in cancer cells triggers mTOR blockade and autophagy. *Cancer Res.* **2013**, *73*, 2247−2258.
(42) Gallyas, F.; Sumegi, B. Mitochondrial Protection by PARP Inhibition. *Int. J. Mol. Sci.* **2020**, *21*, 2767.
(43) Tapodi, A.; Bognar, Z.; Szabo, C.; Gallyas, F.; Sumegi, B.; Hocsak, E. PARP inhibition induces Akt-mediated cytoprotective effects through the formation of a mitochondria-targeted phospho-ATM-NEMO-Akt-mTOR signalosome. *Biochem. Pharmacol.* **2019**, *162*, 98−108.
(44) Mashouri, L.; Yousefi, H.; Aref, A. R.; Ahadi, A. M.; Molaei, F.; Alahari, S. K. Exosomes: composition, biogenesis, and mechanisms in cancer metastasis and drug resistance. *Mol. Cancer* **2019**, *18*, 75.

https://doi.org/10.1021/jasms.1c00215
J. Am. Soc. Mass Spectrom. 2022, 33, 242−250